Chiral logarithms in quenched QCD

Y. Chen,[1,2] S. J. Dong,[1] T. Draper,[1] I. Horváth,[1] F. X. Lee,[3,4] K. F. Liu,[1] N. Mathur,[1] and J. B. Zhang[5]

[1]*Department of Physics and Astronomy, University of Kentucky, Lexington, Kentucky 40506, USA*
[2]*Institute of High Energy Physics, PO Box 918, Beijing 100039, China*
[3]*Center for Nuclear Studies, Department of Physics, George Washington University, Washington, DC 20052, USA*
[4]*Jefferson Lab, 12000 Jefferson Avenue, Newport News, Virginia 23606, USA*
[5]*CSSM and Department of Physics and Mathematical Physics, University of Adelaide, Adelaide, SA 5005, Australia*

The quenched chiral logarithms are examined on a $16^3 \times 28$ lattice with Iwasaki gauge action and overlap fermions. The pion decay constant f_π is used to set the lattice spacing, $a = 0.200(3)$ fm. With pion mass as low as ~ 180 MeV, we see the quenched chiral logarithms clearly in m_π^2/m and f_P, the pseudoscalar decay constant. We analyze the data to determine how low the pion mass needs to be in order for the quenched one-loop chiral perturbation theory (χPT) to apply. With the constrained curve-fitting method, we are able to extract the quenched chiral logarithmic parameter δ together with other low-energy parameters. Only for $m_\pi \lesssim 300$ MeV do we obtain a consistent and stable fit with a constant δ which we determine to be 0.24(3)(4) (at the chiral scale $\Lambda_\chi = 0.8$ GeV). By comparing to the $12^3 \times 28$ lattice, we estimate the finite volume effect to be about 2.7% for the smallest pion mass. We also fitted the pion mass to the form for the re-summed cactus diagrams and found that its applicable region is extended farther than the range for the one-loop formula, perhaps up to $m_\pi \sim 500$–600 MeV. The scale independent δ is determined to be 0.20(3) in this case. We study the quenched non-analytic terms in the nucleon mass and find that the coefficient $C_{1/2}$ in the nucleon mass is consistent with the prediction of one-loop χPT. We also obtain the low energy constant L_5 from f_π. We conclude from this study that it is imperative to cover only the range of data with the pion mass less than ~ 300 MeV in order to examine the chiral behavior of the hadron masses and decay constants in quenched QCD and match them with quenched one-loop χPT.

I. INTRODUCTION

One of the important goals of lattice QCD is to understand, from first principles, low-energy hadron phenomenology as a consequence of chiral symmetry. However, there have been problems with regard to chiral symmetry since the advent of the lattice formulation. The lack of chiral symmetry in traditional approaches (such as Wilson fermions and staggered fermions) leads to a plethora of conceptual and technical difficulties. In particular, as a result of critical slowing down and the existence of exceptional configurations, there is a practical limit on how low in quark (or pion) mass one can carry out a Monte Carlo simulation. The existing calculations with these fermions are typically limited to pion mass greater than ~ 300 MeV. As such, the extrapolation from the current lattice data with pion mass above ~ 300 MeV, sometimes well above, to the physical pion mass of 137 MeV is both a theoretical and a practical challenge. The primary concern is whether the quark mass region (of the lattice data) is inside the range where chiral perturbation theory (χPT) applies. If not, one does not have a reliable analytic form in quark mass dependence to allow for an unbiased extrapolation. Furthermore, most of the quenched χPT calculations are carried out at one-loop order; this limits its range of applicability further, to even smaller quark masses. How small does the quark mass have to be in order to see the chiral behavior predicted by χPT? Is the strange quark in the radius of convergence of χPT? Is there a way to model the chiral extrapolation from well above a 300 MeV

pion mass without introducing systematic errors? These were some of the issues addressed in the panel discussion during the "Lattice 2002" conference [1].

Fortunately, recent progress in lattice fermions has led to formulations (such as domain-wall fermions, overlap fermions, and the fixed-point actions) with lattice chiral symmetry at finite cutoff. As a consequence, many chiral-symmetry relations [2–6] and the quark propagator [7] preserve the same structure as in the continuum. While a lot of progress has been made in checking the chiral symmetries in all these three formulations, we find that overlap fermions [5] offer several distinct advantages. For example, it has been demonstrated that one can simulate near the physical quark-mass region with very gentle critical slowing down [8]. Second, the overlap-fermion inverter can accommodate multiple masses in the calculation of quark propagators [9] and thus is particularly well suited for studying the details of the logarithmically varying mass dependence of physical observables. Third, we find that the $O(a^2)$ and $O(m^2 a^2)$ errors are small [7,8,10]. [There are no $O(a)$ errors due to chiral symmetry [11].] For these reasons, in this paper we use overlap fermions in a quenched lattice calculation to study the chiral logarithms in the pion mass, the pseudoscalar decay constant f_P, the pion decay constant f_π, and the nucleon mass. We determine how small a quark mass or pion mass needs to be for one-loop χPT to be valid. In the present work, we only consider hadrons with degenerate quark masses. Quantities involving the strange quark such as the kaon mass and decay constant will be studied later.

II. NUMERICAL DETAILS

Our calculation is done on a $16^3 \times 28$ lattice with 80 quenched gauge configurations generated with the Iwasaki gauge action [12] at $\beta = 2.264$ and the quark propagators are calculated with overlap fermions. The lattice spacing is 0.200(3) fm, as determined from the pion decay constant $f_\pi(m_\pi)$; the box size is 3.2 fm.

The massive overlap Dirac operator [13] is defined so that at the tree level there is no mass or wave function renormalization [10]:

$$D(m) = \rho + \frac{m}{2} + \left(\rho - \frac{m}{2}\right)\gamma_5 \epsilon(H). \tag{1}$$

Here $\epsilon(H) = H/\sqrt{H^2}$ is the matrix sign function and H is taken to be the Hermitian Wilson-Dirac operator, i.e. $H = H_W = \gamma_5 D_W$. Here D_W is the usual Wilson fermion operator, except with a negative mass parameter $-\rho = 1/2\kappa - 4$ in which $\kappa_c < \kappa < 0.25$. We take $\kappa = 0.19$ in our calculation which corresponds to $\rho = 1.368$.

Throughout the paper, we shall use lattice units for dimensionful quantities, except that the lattice spacing a will be explicit in figures.

Zolotarev approximation

The numerical aspects of the calculation have been given elsewhere [8,10]. The new ingredient is the adoption of the Zolotarev optimal rational approximation [14,15] of the matrix sign function.

To approximate the function $1/\sqrt{x}$, it is suggested [14] that one should consider the minimization of

$$\left\| 1 - \sqrt{x} f(x) \right\|_\infty^{[\lambda_{min}^2, \lambda_{max}^2]}, \tag{2}$$

with $f(x)$ being approximated by a rational polynomial $\tilde{f}(x) \in R^{m-1,m} = p(m-1)/q(m)$ where $p(m-1)$ and $q(m)$ are polynomials with degree $m-1$ and m, respectively. It was proven by Zolotarev [16] that $x\tilde{f}(x^2) \in R^{2m-1,2m}$ is the $\|.\|_\infty$-optimal rational approximation for the sign function on $[-|\lambda_{max}|, -|\lambda_{min}|] \cup [|\lambda_{min}|, |\lambda_{max}|]$. By way of Zolotarev's theorem [16–18], there is an analytic solution

$$\tilde{f}(x) = A \frac{\prod_{l=1}^{m-1}(x + c_{2l})}{\prod_{l=1}^{m}(x + c_{2l-1})}, \tag{3}$$

where the coefficients can be expressed in terms of Jacobian elliptic functions

$$c_l = \frac{sn^2(lK/2m; \kappa)}{1 - sn^2(lK/2m; \kappa)}, \quad l = 1, 2, \ldots, 2m-1, \tag{4}$$

where $\sqrt{1 - \kappa^2} = |\lambda_{max}/\lambda_{min}|$ and K is the complete elliptic integral. According to Ref. [14], A is determined by the condition
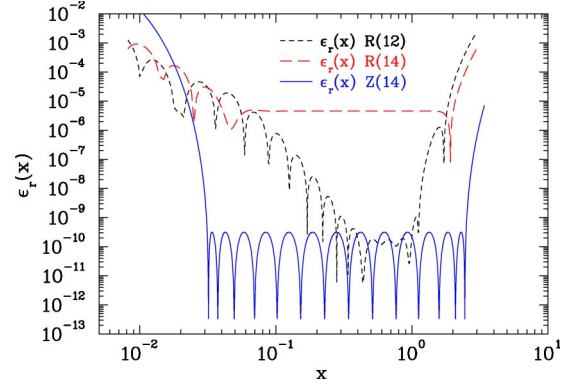

FIG. 1. The residual $\epsilon_r(x)$ of the approximation to the sign function. The solid line is the current 14th degree Zolotarev approximation. The dashed and dotted lines are the 14th [19] and 12th [8] degree Remez approximations respectively.

$$\max_{C[1,(\lambda_{max}/\lambda_{min})^2]} [1 - \sqrt{x}f(x)] = -\min_{C[1,(\lambda_{max}/\lambda_{min})^2]} [1 - \sqrt{x}f(x)]. \tag{5}$$

However, there is a worry when the sign function $\epsilon(H)$ is not bounded by unity because of slight numerical imprecision. From the Cauchy-Schwartz inequality $\|\gamma_5 \tilde{\epsilon}(H)\| < \|\gamma_5\| \|\tilde{\epsilon}(H)\|$, the overlap operator $D(0) = 1 + \gamma_5 \epsilon(H)$ with $\epsilon(H)$ approximated by $\tilde{\epsilon}(H)$ could have superfluous unphysical zero modes [20]. In view of this, we fine-tune the parameter A by reducing it a little from the value determined from Eq. (5) to minimize the positive residual. This doubles the worst residuals.

For the Wilson action kernel $H_W = \gamma_5 D_W$ inside the sign function, the largest eigenvalue is around 2.43 and is fairly stable over the configuration space. Furthermore, we find that the eigenstates of H_W to be projected out become dense at ~ 0.05–0.06. Thus, it is sufficient to specify $\sqrt{1-\kappa^2} = |\lambda_{max}/\lambda_{min}| = 80$. With $|\lambda_{max}| = 2.5$, this gives $|\lambda_{min}|$

TABLE I. Coefficients for the 14th degree Zolotarev approximation in Eq. (6).

i	c_i	q_i
1	0.8371803911435546d−02	0.4203852824188996d−04
2	0.9813674433769438d−02	0.4230339571009471d−03
3	0.1294644813006436d−01	0.1458829357287322d−02
4	0.1831241561050564d−01	0.3894118671815802d−02
5	0.2684553134920763d−01	0.9481580995276351d−02
6	0.4004971283185919d−01	0.2225210303473774d−01
7	0.6031838397347246d−01	0.5146873615634705d−01
8	0.9155798451341547d−01	0.1185868564259925d+00
9	0.1406107013842408d+00	0.2742893835909246d+00
10	0.2211980404641135d+00	0.6437234073136943d+00
11	0.3673892837229880d+00	0.1567367648339766d+01
12	0.6933239005020095d+00	0.4183844803034055d+01
13	0.1812368256185377d+01	0.1442795672202632d+02
14	0.1555827970041009d+02	0.1451886134043600d+03

TABLE II. Pion mass obtained from the $\langle PP \rangle$ correlator on a $16^3 \times 28$ lattice. The pion decay constant f_π is used to set the lattice spacing, $a = 0.200(3)$ fm.

m	m_π	m_π (MeV)	χ^2/N
0.80000	1.3106(42)	1293(20)	0.68
0.60000	1.1069(38)	1092(17)	0.60
0.40000	0.8740(30)	862(13)	0.56
0.32200	0.7743(22)	764(12)	0.54
0.26833	0.7017(24)	692(11)	0.57
0.22633	0.6416(25)	633(10)	0.63
0.18783	0.5829(28)	575(9)	0.72
0.15633	0.5312(31)	524(8)	0.77
0.12950	0.4840(32)	478(8)	0.75
0.10850	0.4438(36)	438(7)	0.70
0.08983	0.4050(38)	400(7)	0.64
0.07583	0.3748(38)	370(7)	0.62
0.06417	0.3470(40)	342(6)	0.58
0.05367	0.3200(43)	316(6)	0.53
0.04433	0.2940(42)	290(6)	0.55
0.03617	0.2693(48)	266(6)	0.52
0.03033	0.2501(54)	247(6)	0.56
0.02567	0.2332(56)	230(7)	0.48
0.02333	0.2244(59)	221(7)	0.58
0.02100	0.2151(61)	212(7)	0.62
0.01867	0.2055(61)	203(7)	0.60
0.01750	0.2005(65)	198(7)	0.64
0.01633	0.1953(69)	193(7)	0.68
0.01400	0.1844(71)	182(8)	0.72

FIG. 2. The pion mass as calculated from the $\langle PP \rangle$ correlator as a function of the bare quark mass m from 0.014 to 0.8. The inset is for the results with small quark masses up to $m = 0.1$.

there should be 29 alternating maxima and minima (including the endpoints of the range) for the approximation with $m = 13$, $n = 14$. As seen in Fig. 1, this feature is preserved with the restriction allowing only positive residuals, as described above.

After partial fraction expansion, the approximated sign function in the rational polynomial $x\widetilde{f}(x^2) \in R^{2m-1,2m}$ has the form

$$\frac{x}{\sqrt{x^2}} \sim x \sum_{i=1}^{N=14} \frac{c_i}{x^2 + q_i}. \tag{6}$$

The coefficients c_i and q_i for our 14th degree Zolotarev approximation are listed in Table I.

In order to improve the approximation of the matrix sign function as well as the convergence in the conjugate gradient inversion in the inner do loop [8–10], it is desirable to project out the lowest several eigenmodes of H_W. We use the Iwasaki improved gauge action which requires that a smaller number of eigenmodes be projected, compared to the Wilson and Lüscher-Weisz gauge actions [21]. We calculated 140 small eigenvalues λ and projected out the lowest 110–140 eigenmodes Ψ_λ, based on the criterion that the residual of the eigenvalue, defined as $||H_W\Psi_\lambda - \lambda\Psi_\lambda||/||\lambda\sqrt{\dim.(H_W)}||$, be less than 10^{-7}. The next smallest eigenvalue is ~ 0.05–0.06, which is well within the window where the approximation for the sign function is better than 3.3×10^{-10}. The residuals of both the inner and the outer do loops for the inversion of the massive overlap Dirac operator in Eq. (1) are at the level of 10^{-7}.

III. PION MASS AND ZERO MODES

We look at the pion mass as calculated from the pseudo-scalar correlator $\langle \Sigma_{\vec{x}} P(\vec{x},t)P(0) \rangle$ where $P = \bar{\psi}i\gamma_5(1 - D/2)\psi$. The pion masses m_π obtained from this correlator

= 0.0315 which is smaller than the largest eigenstates (~ 0.05–0.06) we project out from the kernel H_W. Since the coefficients of the rational polynomial approximation are expressed in terms of the Jacobian elliptic functions, one can use as high a degree of the polynomials as the memory can hold in the multi-mass algorithm. In practice, we use 14th degree which is a sufficiently good approximation for our calculation. We plot the residual $\epsilon_r(x) = x/\sqrt{x^2} - Z_{14}(x)$ for $x > 0$ in Fig. 1 as a function of x. Here $Z_{14}(x)$ is the 14th degree Zolotarev approximation $x\widetilde{f}(x^2)$ from Eq. (2). As we can see, in the selected window [0.031, 2.5], the approximation is better than 3.3×10^{-10}. This is a good deal better than the earlier attempts which approximate $g(x)$ to $1/\sqrt{x}$ with the Remez algorithm, in which case the resultant approximation to the sign function with $xg(x^2)$ is not optimal in the range $[-|\lambda_{max}|, -|\lambda_{min}|] \cup [|\lambda_{min}|, |\lambda_{max}|]$. We plot the residual $\epsilon_r(x)$ for the 14th degree [9] approximation $R(14)$ and 12th degree [8] approximation $R(12)$ with the Remez method in comparison with the 14th degree Zolotarev approximation $Z(14)$. We see that the Remez method gives residuals in the order of 10^{-5} in the relevant range [0.031, 2.5]. We note that according to Chebyshev's theorem, the errors of the optimal rational approximation $\widetilde{f}(x) \in R^{m,n} = p(m)/q(n)$ have $m + n + 2$ alternating signs in the range of the approximation. Since the Zolotarev approximation to the sign function is optimal, it should satisfy this requirement. In other words,
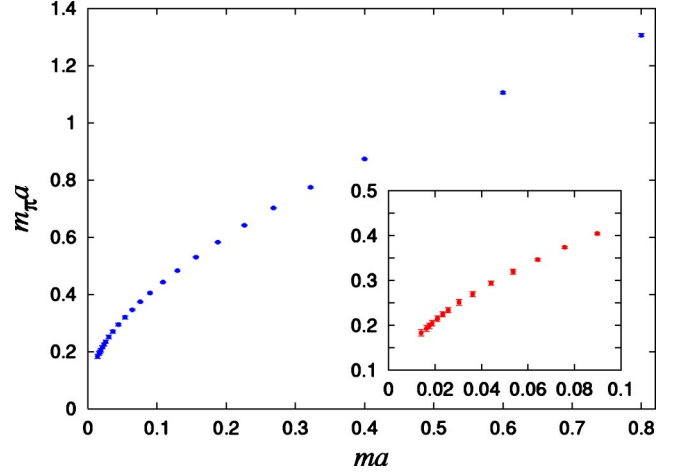
are listed in Table II and plotted in Fig. 2 as a function of the quark mass m. Our smallest pion mass is 182(8) MeV.

Consider the contributions of the zero modes to the meson correlator of the interpolation field $M = \bar{\psi}\Gamma(1 - D/2)\psi$:

$$\int d^3x \langle M(x)M^\dagger(0)\rangle|_{zero\ modes} = -\int d^3x \left[\sum_{i,j=zero\ modes} \frac{\langle \mathrm{tr}[\psi_j^\dagger(x)\gamma_5\Gamma\psi_i(x)]\mathrm{tr}[\psi_i^\dagger(0)\bar{\Gamma}\gamma_5\psi_j(0)]\rangle}{m^2} \right.$$

$$\left. + 2\sum_{i=0,\lambda>0} \frac{\langle \mathrm{tr}[\psi_\lambda^\dagger(x)\gamma_5\Gamma\psi_i(x)]\mathrm{tr}[\psi_i^\dagger(0)\bar{\Gamma}\gamma_5\psi_\lambda(0)]\rangle}{\lambda^2 + m^2} \right], \tag{7}$$

where Γ is the spinorial matrix and $\bar{\Gamma} = \pm\Gamma^\dagger$. For the pseudoscalar case with $\Gamma = \gamma_5$, the zero modes contribute to both the direct and cross terms in the correlator. They contribute also to the cross terms in the $\langle \Sigma_{\vec{x}} A_4(\vec{x},t)P(0)\rangle$ and $\langle \Sigma_{\vec{x}} A_4(\vec{x},t)A_4(0)\rangle$ correlators, where $A_4 = \bar{\psi}i\gamma_4\gamma_5(1 - D/2)\psi$, but not to the direct terms. In view of the worry that the pseudoscalar correlator may be contaminated by the zero modes [10,22] particularly at small volumes, we look at $\langle \Sigma_{\vec{x}} A_4(\vec{x},t)A_4(0)\rangle$ to check if the masses calculated are the same as those from the $\langle PP\rangle$ correlator. We plot the ratios of the pion masses from the $\langle PP\rangle$ correlator and the $\langle A_4A_4\rangle$ correlator in Fig. 3. We see that the ratios are basically unity within errors all the way to the smallest quark mass. This suggests that at this volume, i.e. $V = (3.2\mathrm{fm})^4$, there is no detectable contamination due to the zero modes. However, this is not so at smaller volumes. We will show results on the $12^3 \times 28$ lattice and discuss the volume dependence in Sec. V.

It has been shown that the correlator $\langle PP\rangle - \langle SS\rangle$ can get rid of the zero mode contribution [22] for both the direct and cross terms. This is a good procedure for medium quark masses. For small quark masses, there is a complication due to the quenched η'-π ghost state contribution in the $\langle SS\rangle$ [23] which has a mass close to 2 times the pion mass. We have fitted the $\langle PP\rangle - \langle SS\rangle$ correlator with the inclusion of the ghost state which has a negative weight. We show in
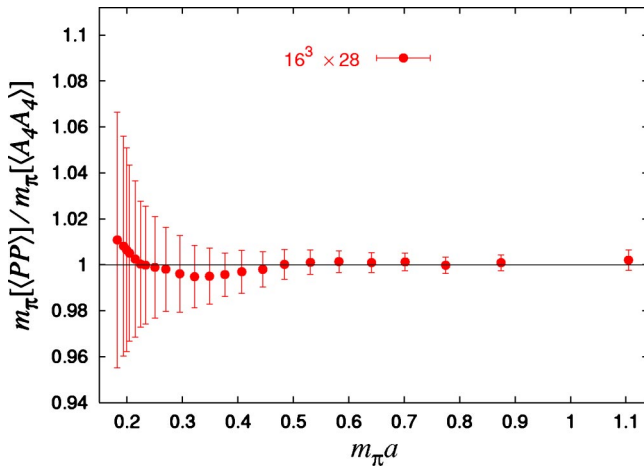
Fig. 4 the ratio of pion masses determined from the $\langle PP\rangle$ and the $\langle PP\rangle - \langle SS\rangle$ correlators. We note that the errors from the $\langle PP\rangle - \langle SS\rangle$ are larger for $m_\pi \lesssim 0.4438(36)$ due to the presence of the ghost state which is close to the ground state pion mass. It is not clear to what extend the additional complication due to the ghost state is disentangled from that of the zero modes. In any case, we find that the pion masses obtained are consistent with those from the $\langle PP\rangle$ and $\langle A_4A_4\rangle$ correlators. Their central values differ by 2.5% at most. We will come back to this issue in the next section when we fit the quenched chiral logarithm in m_π.

IV. CHIRAL LOGARITHM IN m_π

It is predicted that in the quenched approximation, there are quenched chiral logarithms [24,25] arising from the hairpin diagrams; the flavor-singlet pseudoscalar correlator does not yield a full η' mass due to the absence of dynamical fermion loops. Instead, the would-be η' propagator gives a double pole of the Goldstone boson. The predicted form for the one-loop formula in χPT is [26,27]

$$m_\pi^2 = Am\{1 - \delta[\ln(Am/\Lambda_\chi^2) + 1]\} + A_\alpha m^2[1 + 2\ln(Am/\Lambda_\chi^2)] + Bm^2, \tag{8}$$

FIG. 3. Ratio of pion masses as calculated from the $\langle PP\rangle$ and $\langle A_4A_4\rangle$ correlators as a function of the m_π obtained from the $\langle A_4A_4\rangle$ propagator.
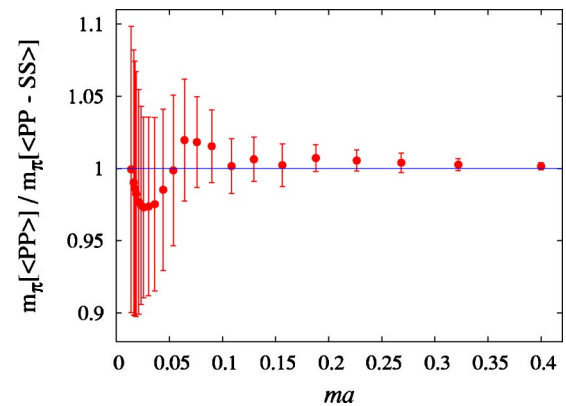
FIG. 4. Ratio of pion masses as calculated from the $\langle PP\rangle$ and $\langle PP\rangle - \langle SS\rangle$ correlators as a function of the *ma*.

TABLE III. Summary of the quenched chiral logarithmic calculations in m_π^2 with different fermion actions and ranges of quark masses. $m_{\pi,min}$ is the minimum pion mass used in the fitting. $m_{\pi,trou}$ is the pion mass at the trough of m_π^2/m. $\mathcal{E}$ is the percentage of excess of the highest m_π^2/m at $m_{\pi,min}$ relative to the corresponding trough at $m_{\pi,trou}$.

Group	Fermion	La (fm)	$m_{\pi,min}$ (MeV)	$m_{\pi,trou}$ (MeV)	$\mathcal{E}$	δ
CP-PACS [28]	Wilson	3.2	300	~550	~8%	0.060(10)–0.106(5)
Fermilab [29]	Wilson-Clover	2.7	290	~400	~7%	0.073(20)
QCDSF [30]	Wilson-Clover	1.5–2.3	400	~800	~11%	0.14(2)
MILC [31]	Staggered	2.6	320	~700	~8%	0.061(3)
Kim and Ohta [32]	Staggered	2.6	210	~570	~8%	0.057(13)
Blum et al. [22]	Domain Wall	3.2	390	~740	~11%	0.07(4)
RCB [33]	Domain Wall	2.4	285	~660	~6%	0.107(38)
BGR [34]	fixed point	2.6	210	~870	~15–20%	0.17(2)
BGR [34]	Chirally Improved	2.4	240	~930	~15–20%	0.18(3)
Chiu and Hsieh [35]	Overlap	1.5	440	~770	~11%	~0.2
Present work	Overlap	3.2	182	~480	~33%	0.236(33)(37) (one loop) 0.20(3) (cactus)

where the coefficients A, A_α and B are given in terms of the parameters Σ, f, α_Φ and $2\alpha_8 - \alpha_5$ in the quenched effective chiral Lagrangian, i.e.

$$A = 2\Sigma/f^2,$$

$$A_\alpha = \frac{\alpha_\Phi A^2}{3(4\pi f)^2},$$

$$B = \frac{(2\alpha_8 - \alpha_5)A^2}{(4\pi f)^2}, \tag{9}$$

and Λ_χ is an unphysical cutoff scale which is usually taken in χPT to be in the range of 0.5–1.0 GeV. The parameter α_Φ is the singlet coupling in the quenched theory. The quenched chiral logarithmic parameter δ is

$$\delta = \frac{m_0^2}{16\pi^2 N_f f^2}, \tag{10}$$

where $m_0 \sim 870$ MeV from the Veneziano model of the η' mass. From this, one estimates that $\delta = 0.183$.

There are several calculations to extract the chiral logarithmic parameter δ [22,28–35]. Save for Refs. [34,35], most of the calculations obtained values for δ in the range 0.06–0.1 which are smaller than the expectation. We have summarized these results in Table III. The present simulation adopts the overlap fermion action which has exact chiral symmetry on the lattice and a highly accurate numerical approach (the matrix sign function is approximated to better than 10^{-9}). This should be a valuable tool to probe the relevant range of applicability of the one-loop χPT with pion mass as low as ~ 180 MeV on a fairly large volume (3.2 fm). We plot in Fig. 5 the $\langle PP \rangle$ results for m_π^2/m as a function of the bare quark mass m. We see clearly that below $m = 0.1295$ ($m_\pi \sim 480$ MeV), there is a dramatic divergent

behavior. The ratio of the highest value at $m = 0.014$ ($m_\pi \sim 180$ MeV) to that at the trough at $m = 0.1295$ ($m_\pi \sim 480$ MeV) is ~ 1.33. Thus, the percentage excess, $\mathcal{E}$, of the highest value at the minimum pion mass $m_{\pi,min}$ relative to that at the trough at $m_{\pi,trou}$ is 33%. Most of the calculations studying the quenched chiral log stopped above $m_\pi \sim 300$ MeV; thus, they seem to be seeing the onset of this behavior with corresponding excess $\sim 6\%$–11%. In Table III, we summarize the attempts made by various groups to calculate this quenched chiral log from m_π^2/m with different actions and lattices. Except for the present work, all the results are fitted to Eq. (8) without the A_α term.

We see from Table III that the results are not consistent with each other. There is a large spread in δ and $m_{\pi,trou}$ which invokes many issues to ponder: To what extent does the fermion action matter? Is χPT valid in the range of pion masses calculated? If so, is the one-loop formula sufficient and how does one judge it? The parameters A, δ, Λ_χ, and B are not linearly independent in Eq. (8); how does one fit them? Practically all the calculations so far ignored A_α; does it change the results much if included? How large are the finite volume effects for the range of pion masses in the
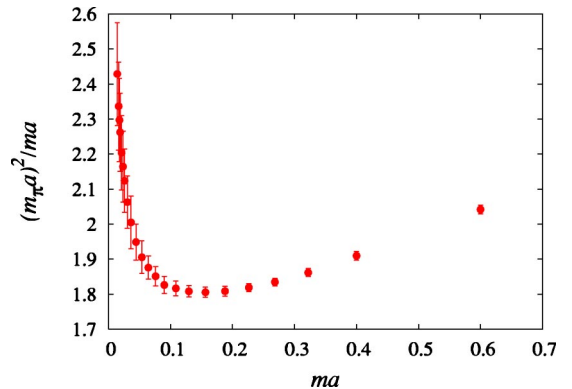

FIG. 5. The ratio m_π^2/m as a function of the quark mass m.

TABLE IV. The low-energy chiral parameters C_1 and C_{1L} (and C_2 and C_{2L}) are fitted from Eq. (11) with a maximum of 17 quark masses in correlated and constrained fits for several ranges of quark masses with the minimum quark mass at 0.0140 [which corresponds to the smallest pion mass at 182(8) MeV]. These are then used to determine A, δ, A_α, and B from Eq. (12). The parameters A, δ, and B vary with the chiral scale, and are evaluated at $\Lambda_\chi = 0.8$.

m_{max}	$m_{\pi,max}$	C_1	C_{1L}	A	δ	A_α	B	χ^2/dof
0.02100	0.2151(61)	0.82(17)	$-0.368(64)$	1.51(27)	0.244(40)	–	–	0.48
0.02333	0.2244(59)	0.84(16)	$-0.362(52)$	1.51(24)	0.239(36)	–	–	0.49
0.02567	0.2332(56)	0.83(15)	$-0.353(51)$	1.48(23)	0.238(35)	–	–	0.46
0.03033	0.2501(54)	0.84(14)	$-0.350(56)$	1.48(23)	0.236(35)	–	–	0.44
0.03617	0.2693(48)	0.85(15)	$-0.349(50)$	1.49(22)	0.234(33)	–	–	0.42
0.04433	0.2940(42)	0.87(14)	$-0.340(50)$	1.50(22)	0.226(31)	–	–	0.46
0.05367	0.3200(43)	0.87(14)	$-0.315(47)$	1.44(21)	0.219(32)	–	–	0.58
0.06417	0.3470(40)	1.05(16)	$-0.256(50)$	1.53(22)	0.167(30)	–	–	0.61
0.07583	0.3748(38)	1.08(16)	$-0.246(48)$	1.55(21)	0.159(29)	–	–	0.64
0.08983	0.4050(38)	1.13(16)	$-0.233(42)$	1.57(21)	0.148(26)	$-0.003(167)$	1.55(55)	0.82
0.10850	0.4438(36)	1.16(14)	$-0.227(42)$	1.59(19)	0.143(24)	$-0.053(132)$	1.39(45)	0.93
0.12950	0.4840(32)	1.14(13)	$-0.228(39)$	1.58(18)	0.145(22)	$-0.092(125)$	1.42(40)	0.92
0.15633	0.5312(31)	1.16(12)	$-0.228(39)$	1.60(17)	0.143(21)	0.003(93)	1.42(31)	0.79
0.18783	0.5829(28)	1.15(9)	$-0.230(38)$	1.59(13)	0.145(19)	$-0.001(63)$	1.43(24)	0.79
0.22633	0.6416(25)	1.15(8)	$-0.221(35)$	1.57(12)	0.141(17)	$-0.093(49)$	1.47(18)	0.81
0.26833	0.7017(24)	1.16(8)	$-0.221(31)$	1.58(11)	0.140(16)	$-0.046(38)$	1.44(15)	0.95
0.32200	0.7743(22)	1.17(8)	$-0.214(30)$	1.58(11)	0.135(15)	$-0.070(40)$	1.43(14)	0.95
0.40000	0.8740(30)	1.17(7)	$-0.213(30)$	1.58(11)	0.135(15)	$-0.079(37)$	1.43(13)	0.92

calculation? (As will be demonstrated in Sec. V, the pion masses calculated from the $\langle PP \rangle$ correlator in small volumes are contaminated by the zero modes even up to fairly large quark masses, i.e. the strange quark region. This could affect the position of $m_{\pi,trou}$ and the result for δ.) How does one control the finite volume and zero mode effects?

Before addressing these questions, we first point out that there is a fundamental problem in the way the lattice data are usually fitted to the form predicted by the χPT. The common practice is to fit the lattice data to the χPT result from a high pion mass down to cover the range of calculated masses and then extrapolate to the physical pion mass. This can force a fit but cannot answer the question as to whether the one-loop chiral formula is applicable for the range of masses considered. It is possible that the range of masses will require higher orders in χPT or even that the mass range is outside the radius of convergence of χPT. Then one does not know the precise form to fit. Extrapolating down from the pion mass as high as 1 GeV is simply diametrically opposed to the philosophy of χPT which is based on the expansion of small quark masses and momenta.

So how does one proceed? To be consistent with the χPT approach, we start from the smallest quark mass and ask where the one-loop formula applies [36]. Since we have come down to the pion mass as low as ~ 180 MeV, we will assume that it is in the range where one-loop χPT is valid. We fit the one-loop formula with the five smallest pion masses and then incrementally add higher pion masses one by one. If the formula is valid for the range of masses, then the parameters will remain constant; i.e., they are truly the low energy constants that we seek to evaluate. On the other hand, if the parameters begin to change as one includes more

higher masses, we take it as an indication that the one-loop formula starts to lose its applicability. This could be due to the fact that higher orders are needed or that the mass is simply outside the range of validity of χPT.

We mentioned earlier that in the fitting of the one-loop formula, the parameters A, δ, Λ_χ, and B are not linearly independent. We can rewrite Eq. (8) as

$$m_\pi^2 = C_1 m + C_{1L} m \ln(m) + C_2 m^2 + C_{2L} m^2 \ln(m), \quad (11)$$

where

$$C_1 = A[1 - \delta(\ln A - 2 \ln \Lambda_\chi + 1)],$$

$$C_{1L} = -A\delta,$$

$$C_2 = A_\alpha(1 + 2 \ln A - 4 \ln \Lambda_\chi) + B,$$

$$C_{2L} = 2A_\alpha \quad (12)$$

are the independent parameters. Therefore, we have one redundant variable which we take to be the cutoff scale Λ_χ. We adopt a Bayesian-based constrained curve-fitting method [37,38] with an adaptive procedure to obtain priors sequentially according to the relative importance of the parameters. The details of the constrained curve-fitting algorithm for the hadron masses will be given elsewhere [39]. In each of the quark mass ranges, the priors for C_1, C_{1L}, C_2, and C_{2L} are obtained from the corresponding $\langle A_4 A_4 \rangle$ correlators. After the C parameters are determined from the fit, we solve Eq. (12) to obtain A, δ, A_α, and B for a given Λ_χ. We list their results evaluated at $\Lambda_\chi = 0.8$ together with C_1 and C_{1L} in Table IV. We also plot A, A_α, B, and δ as a function of the
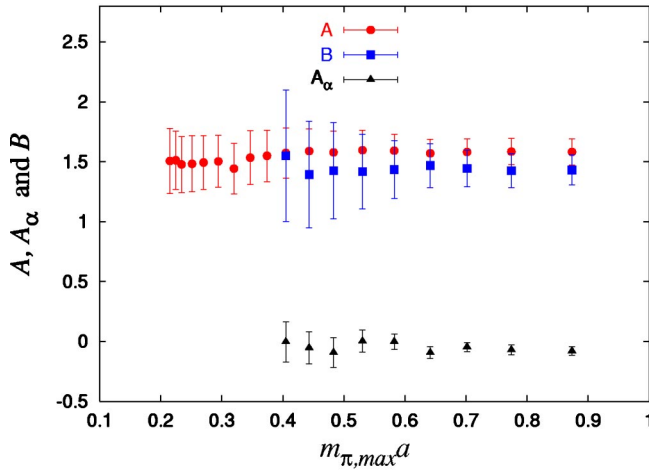
FIG. 6. Fitted A, A_α, and B as a function of $m_{\pi,max}$, the maximum pion mass of the fit, for $\Lambda_\chi = 0.8$. The minimum pion mass is at 0.1844(71) [182(8) MeV].

FIG. 8. Fractional contributions for different terms in Eq. (11). The input of the C parameters are from the fit with $m_{max} = 0.03617$. Note the combined contribution $C_1 m^2 + C_{1L} m^2 \ln(m)$ denoted by the dashed line is very small.

maximum pion mass $m_{\pi,max}$ of the fitting range in Figs. 6 and 7. We should mention that due to the limited number of gauge configurations, we are not able to carry out correlated fits with a reasonable χ^2 for more than 17 quark masses. Therefore, for longer ranges, we choose a maximum of 17 representative masses to cover the range of the fit. For m_{max} less than 0.08983 [$m_\pi = 0.4050(38)$ or 400(7) MeV], we find that the data are dominated by C_{1L} and C_1. The contributions from C_2 and C_{2L} cancel each other and the combined contribution is negligible compared to those of C_{1L} and C_1. This is illustrated in Fig. 8 for a typical fit. As a result, it is practically impossible to obtain a reliable fit for C_2 and C_{2L}. We decided to fit these low mass data using a prior for C_{2L} which is limited to less than 2 during the fitting procedure for

FIG. 7. The solid circles are the quenched chiral δ plotted as a function of $m_{\pi,max}$, the maximum pion mass of the fitting range, with the minimum pion mass fixed at 0.1844(71) [182(8) MeV]. The open circles [solid squares] are those fitted downward from a maximum pion mass fixed at 0.8740(30) [862(13) MeV] (0.6414(21)[633(10) MeV]) and plotted as a function of $m_{\pi,min}$, the minimum pion mass of the fitting range. These results are at $\Lambda_\chi = 0.8$.
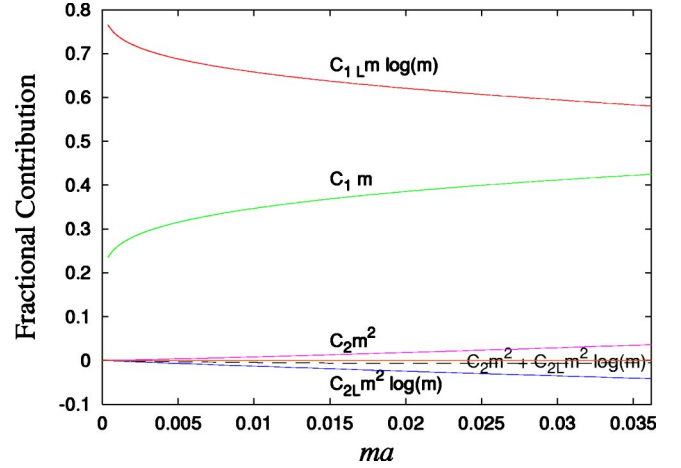
the $\langle A_4 A_4 \rangle$ correlators. We tried using the priors without such a limit and also tried dropping C_2 and C_{2L} all together in these low mass ranges and found that the fitted C_1 and C_{1L} are not changed within errors. The central values for δ are changed only by 1%–2%. In view of this inability to fit C_2 and C_{2L}, we do not quote the fitted A_α and B below $m_{max} = 0.08983$ [$m_\pi = 0.4050(38)$] where the errors are larger than their central values. Hopefully, with better statistics, one will be able to extract the parameters A_α and B in the range $m_\pi < 400(7)$ MeV.

We see in Fig. 6 that values for A are fairly stable throughout the range of the fit. A_α and B are also stable in the range where $m_{max} \gtrsim 0.08983$ and A_α is consistent with zero in this range. On the contrary, δ in Fig. 7 is constant up to $m_{max} \sim 0.044$ which corresponds to $m_{\pi,max} \sim 300$ MeV. Beyond that, it has a sharp drop. We take the fact that δ is sensitive to the range of masses as an indication that the one-loop chiral formula in Eq. (8) is valid *only* up to $m_\pi \sim 300$ MeV. Below this value, the parameters in the formula do not exhibit mass dependence and thus they are the low energy constants of the effective chiral theory at a certain chiral scale (e.g. $\Lambda_\chi = 0.8$).

Next, we simulate what has been commonly done in lattice calculations. We fix the maximum pion mass at $m_\pi = 0.8740(30)$[862(13) MeV] and incrementally include lower pion masses to fit Eq. (11). We find that no matter how many low pion masses are included, the results are not compatible with those starting from $m_{\pi,min} = 0.1844(71)$ [182(8) MeV] and ending at $m_{\pi,max} \sim 300$ MeV. We illustrate this by plotting, in Fig. 7, the fitted δ (open circles) as a function of the minimum pion mass $m_{\pi,min}$ for the range of the fit. We see that when pion masses down to 300–400 MeV are included, the fitted δ is in the range of ~ 0.15 which is consistent with those found in Table III with a similar mass range and can explain why most of the calculations end up with a small δ. The only exception is Ref. [35] which obtains a large $\delta \sim 0.2$ with $m_{\pi,min} \sim 440$ MeV. We speculate that this may be due to the small volume used ($L = 1.5$ fm). As will be explored further in Sec. V, we find that
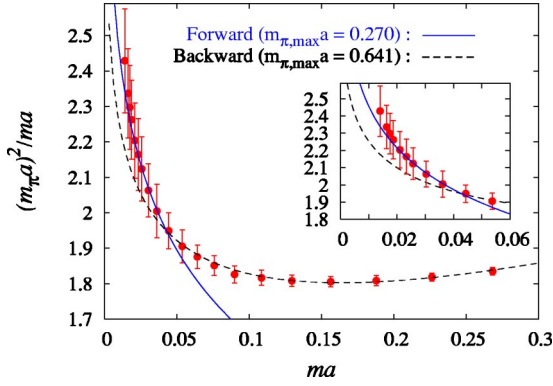
FIG. 9. The fit to m_π^2/m as a function of the quark mass m. The solid line is the forward fitting ending at $m_\pi = 0.269(5)(m = 0.03617)$. The dashed line is the backward fitting from $m_\pi = 0.641(2)(m = 0.22633)$ to the smallest quark mass. The inset is a blowup for the small quark mass region.

the zero modes make a sizable contribution to pion masses as high as 800 MeV on a lattice with $L = 2.4$ fm and likely higher at smaller volumes. It would be sensible to check if this is the case by comparing pion masses obtained from the $\langle PP \rangle$ correlator to those from $\langle A_4 A_4 \rangle$ as will be done in Sec. V.

In view of the fact that the rise of m_π^2/m left of the trough at $m_\pi \sim 480$ MeV is mostly due to the chiral logarithm while the rise right of the trough is mostly due to the m^2 term, we first fit the points around the trough (i.e. from $m = 0.07583$ to 0.22633) with the form in Eq. (11) but without the A_α term and then extend the range by including smaller quark masses. The results of A, δ and B turn out to be very close to the ones starting from the maximum pion mass at $m_\pi = 0.8740(30)[862(13)$ MeV$]$. We show the results of δ (labeled δ_{trou}) as a function of the minimum pion mass $m_{\pi,min}$ in Fig. 7 and find them almost the same as δ_{min} at small quark masses and similarly smaller than those where the pion masses are restricted to lower than ~ 300 MeV.

For comparison, we show in Fig. 9 the fit of m_π^2/m for the forward fitting ending at $m_\pi = 0.269(5)(m = 0.03617)$ (solid line) and the backward fitting from $m_\pi = 0.641(2)(m = 0.22633)$ to the smallest quark mass (dashed line).

As one can see from Eq. (12), the parameters A, δ, and B depend logarithmically on Λ_χ. In Fig. 10 we show how A and δ vary as a function of Λ_χ. The C_1 and C_{1L} are taken from the fit for $m_{max} = 0.03617$ $[m_\pi = 0.2693(48)$ or $266(6)$ MeV$]$ in Table IV. Incidentally, for a given C_1 and C_{1L}, there is a maximal value

$$\Lambda_{\chi,max} = \sqrt{C_{1L}} e^{C_1/2C_{1L}} \qquad (13)$$

(for which $\delta = 1$ and $A = C_1$), beyond which no solution exists. But this is well beyond the range of applicability of Eq. (8). We should point out that the fact A runs with $\ln \Lambda_\chi$ is a peculiar feature of quenched QCD. This is not the case in full QCD where A is basically the quark condensate where there is no quenched chiral δ [24]. From Eq. (12), we see that the combination $A\delta$ is independent of the chiral scale. This makes δ also run with $\ln \Lambda_\chi$. This is not physical, but rather
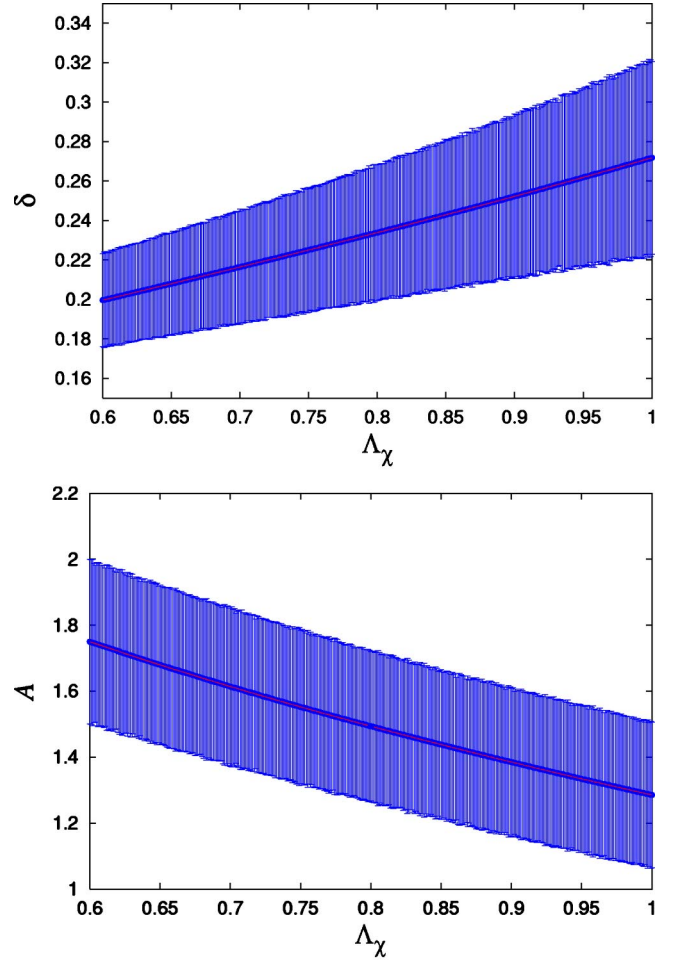

FIG. 10. The running of δ and A and as a function of Λ_χ according to the one-loop formula. The input of C_1 and C_{1L} are for the fit with $m_{max} = 0.03617$.

is due to the fact that Eq. (8) contains only the leading term in the expansion of δ [40]. To see this, consider the example where the leading logarithm is re-summed for the "cactus diagrams" [24] (one is not concerned with A_α and B here) which leads to

$$m_\pi^2 = m^{1/(1+\delta)} (A\Lambda_\chi^{2\delta})^{1/(1+\delta)}. \qquad (14)$$

We see that the m and Λ_χ dependence of δ are separable which implies that δ does not run with Λ_χ, and the unphysical Λ_χ can be absorbed in A with

$$A \propto \Lambda_\chi^{-2\delta}, \qquad (15)$$

which gives

$$\frac{d \ln A}{d \ln \Lambda_\chi^2} = -\delta. \qquad (16)$$

This is the same as obtained from Eq. (8) when one requires that m_π^2 be independent of Λ_χ and assumes that δ does not depend on Λ_χ.

We shall report our final results based on the fit of pion mass from $0.184(7)(m = 0.014)$ to $0.269(5)(m = 0.03617)$

TABLE V. The low energy parameters in the quenched chiral Lagrangian are given as a fit of Eq. (11) from $m = 0.014$ [$m_\pi = 182(8)$ MeV] to $m = 0.03617$ [$m_\pi = 266(6)$ MeV] at $\Lambda_\chi = 0.8$ GeV. The second error in δ is the estimated systematic error determined as the average deviation at $\Lambda_\chi = 1$ and 0.6 GeV from the value at 0.8 GeV.

Λ_χ	A	δ
0.8 GeV	1.46(22) GeV	0.236(33)(37)

with 9 quark masses. This choice is based on the observation that δ begins to decrease beyond $m_{max} = 0.03617$ [$m_{\pi max} = 0.269(5)$]. Although this happens to coincide with the minimum in χ^2/N_{DF} in Table IV, we should stress that a minimal χ^2/N_{DF} is not and should not be the criterion for such a choice. As we pointed out earlier, the primary difficulty in chiral extrapolation is the uncertainty about the valid range of one-loop formula in χPT. A χ^2/N_{DF} less than unity does not imply that the fitting formula is correct. One way to judge is the criterion that we adopt; namely, the one-loop formula is not valid when the fitted parameters do not remain constant beyond certain $m_{\pi max}$.

As we said earlier, we are not able to obtain a reliable fit for A_α, and B at these low masses. As for the finite volume systematic errors, we note that the finite volume correction for the lowest m_π^2 is estimated to be 5.4% and the second lowest m_π^2 is estimated to be 3.6%. (This will be explained in more detail in Sec. V.) We thus estimate the systematic errors due to the finite volume to be at the few percent level which are smaller than our current statistical errors. We also dropped the last quark mass and fitted the 8 quark masses from $m = 0.01633$ [$m_\pi = 0.195(7)$] to $m = 0.03617$ [$m_\pi = 0.269(5)$] and found that A and δ change only about 1%, which are much smaller than the statistical errors.

We quote our final results for the low-energy parameters of the quenched one-loop chiral perturbation theory at $\Lambda_\chi = 0.8$ GeV close to the ρ mass in Table V. In view of the unphysical dependence of δ on Λ_χ at the order specified in Eq. (8), we shall estimate the systematic error to be the average deviation from the value at 0.8 GeV of the values at $\Lambda_\chi = 1$ GeV and 0.6 GeV. We see that the central value of δ is somewhat larger than the phenomenological value of 0.183 in Eq. (10), but they are consistent within errors.

Fitting of re-summed cactus diagrams

Since at small quark masses, the higher order results with $[\delta \ln(m)]^n$ corrections are important, it is pertinent to fit the re-summed cactus diagram form [24] for the chiral logarithm, which leads to a scale independent δ. Thus, we shall fit with the power form

$$m_\pi^2 = A m^{1/(1+\delta)} + B m^2. \tag{17}$$

Similar to fitting the one-loop formula in Eq. (11), we start from the smallest quark mass and fit upward first. Since at very small quark masses the B contribution is very small, we put a very weak constraint at 1.8 ± 1 which covers the
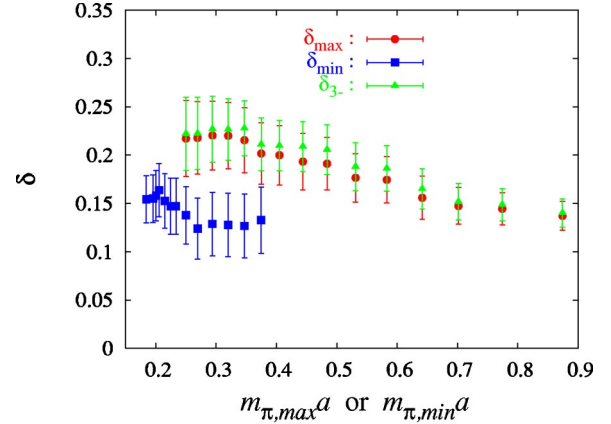

FIG. 11. The solid circles are the scale independent chiral δ plotted as a function of $m_{\pi,max}$, the maximum pion mass of the fitting range, with the minimum pion mass fixed at 0.1844(71) [182(8) MeV]. The same are for the triangles (δ_{3-}) except the starting minimum pion mass is at 0.2055(61) [203(7) MeV]. The solid squares are those fitted downward from a maximum pion mass fixed at 0.6416(25) [633(10) MeV] and plotted as a function of $m_{\pi,min}$, the minimum pion mass of the fitting range.

range of B as fitted in one-loop formula in Table IV. The resultant δ, A and B are presented in Figs. 11, 12, and 13. We see that, in contrast to the sharp transition at $m_{\pi,max} \sim 300$ MeV in the one-loop formula fit, the transition for δ is smoother. The behavior for A and B are similarly changed. This is to be expected, since the power form takes into account the re-summed cactus diagrams to all orders. As such, it should extend the range of applicability of the quenched χPT to beyond $m_\pi \sim 300$ MeV for the one-loop case, provided that it dominates the higher loop corrections. From the fitted results, it appears that the power form gives a stable fit to the trough of m_π^2/m and is perhaps valid to $m_\pi \sim 500$–600 MeV. Above $m_\pi \sim 640$ MeV, all the parameters (δ, A and B) are different from those below $m_{\pi,max} \sim 300$–400 MeV by two sigmas. We shall quote the result of the scale independent δ at $m = 0.08083$ [$m_\pi = 400(7)$ MeV] where $\delta = 0.20(3)$. We have fitted also the
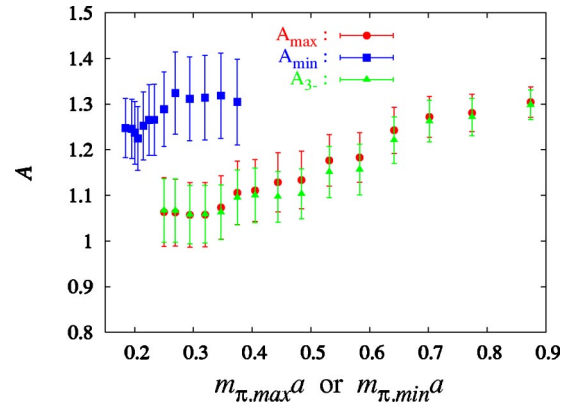

FIG. 12. The circles and triangles are fitted A as a function of $m_{\pi,max}$ starting from $m = 0.014$ and 0.01867, respectively. The squares are those fitted downward starting from $m = 0.22633$ as a function of $m_{\pi,min}$.
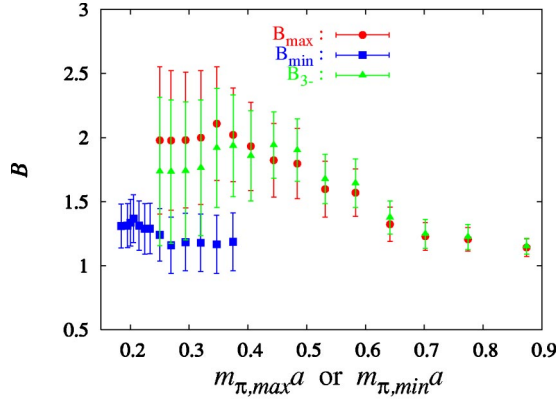
FIG. 13. The circles and triangles are fitted B as a function of $m_{\pi,max}$ starting from $m = 0.014$ and 0.01867, respectively. The squares are those fitted downward starting from $m = 0.22633$ as a function of $m_{\pi,min}$.

pion mass from the $\langle PP - SS \rangle$ correlator and find that the changes of δ and A are small, at a few percent level. In the range between $m_\pi = 0.2501(54)$ and $0.4840(32)$, the change is at the 1% level. For example, $\delta = 0.20(4)$ at $m = 0.08083(m_\pi = 400(7)$ MeV).

We also fitted the points around the trough ($m = 0.07583 - 0.22633$) and then incrementally added smaller quark masses in the fit, as we did for the one-loop formula. The results are plotted in Figs. 11, 12, and 13 as a function of $m_{\pi,min}$ and labeled δ_{min}, A_{min} and B_{min}. We see again that they do not reproduce those parameters which are obtained from fitting the range from $m = 0.014$ to 0.08983 [$m_\pi = 0.4050(38)$].

As we are concerned about the finite volume effect (this will be addressed in Sec. V) for small quark masses, we drop the three smallest quark masses and then fit the pion mass upward. We plot the results in Figs. 11, 12, and 13 as a function of $m_{\pi,max}$ and labeled δ_{3-}, A_{3-} and B_{3-}. We see that in most cases they are only a few percent different from those (δ_{max}, A_{max} and B_{max}) without dropping the last three quark masses. We have also performed the same test for the one-loop logarithmic formula fit and find that the parameters are also not changed much. We plot in Fig. 14 the results of δ_{3-} from this fit together with δ_{max} as obtained from the one-loop log fit without dropping the last 3 points. We see that the characteristic transition around $m_\pi \sim 300$ MeV is still visible.

V. FINITE VOLUME EFFECTS

Intertwined in the discussion of the validity of the one-loop χPT for a certain mass range are the finite volume effects. There are two questions to consider: First of all, how does one know how large the zero mode contributions are, and how much do they affect the pion mass in the range of the fitting? Secondly, how large is the finite volume effect for the pion mass where the finite box is not larger than 4 times the Compton wavelength of the pion? We considered the zero mode contribution in Sec. III where we examined the ratio of pion masses from the $\langle PP \rangle$ and $\langle A_4 A_4 \rangle$ correlators
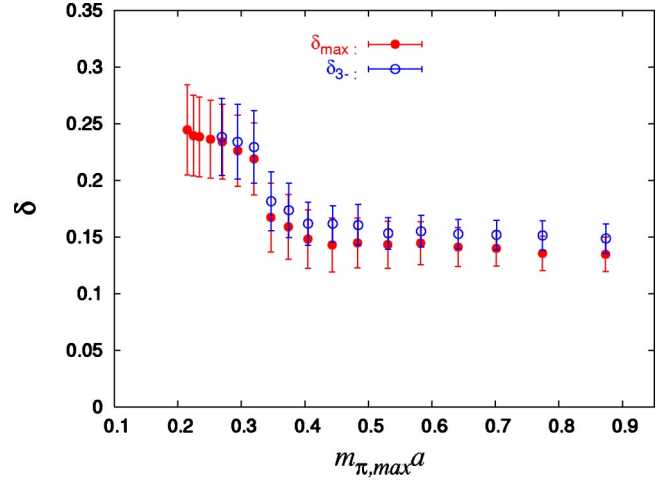

FIG. 14. The solid circles are the chiral δ (δ_{max}) plotted as a function of $m_{\pi,max}$, the maximum pion mass of the fitting range, with the minimum pion mass fixed at $0.1844(71)$ [$182(8)$ MeV]. The same are for the open circles (δ_{3-}) except the starting minimum pion mass is at $0.2055(61)$ [$203(7)$ MeV].

for the $16^3 \times 28$ lattice and found that the ratio is basically unity within errors for the range of quark masses that we are concerned with. We now look at the same ratio in a smaller lattice $12^3 \times 28$ ($La = 2.4$ fm in this case). They are plotted in Fig. 15 together with those from the $16^3 \times 28$ lattice. We see that the ratio for the $12^3 \times 28$ lattice deviates from unity by two sigmas for pion mass in the range of 0.5–0.8 or ~ 500–800 MeV. The central value of the ratio goes down to 98% at $m_\pi \sim 300$ MeV before it turns back to around unity for small pion mass due to the finite volume effect. This is a clear indication that the zero mode contribution to the $\langle PP \rangle$ propagator is visible even for pion mass as heavy as ~ 800 MeV. Most of the calculations compiled in Table III have volumes similar to our $12^3 \times 28$ lattice, therefore one needs to be concerned about the zero mode contamination which is a finite volume artifact. Since the zero mode contribution varies as $1/\sqrt{V}$ [10,22], the effect of the zero mode contribution will be larger for calculations with still smaller
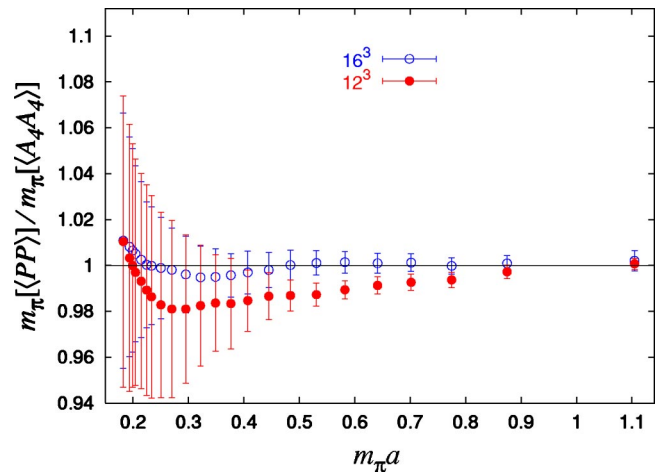

FIG. 15. Ratio of pion masses as calculated from the $\langle PP \rangle$ and $\langle A_4 A_4 \rangle$ correlators as a function of m_π from the $\langle A_4 A_4 \rangle$ correlator for both the $16^3 \times 28$ and $12^3 \times 28$ lattices.
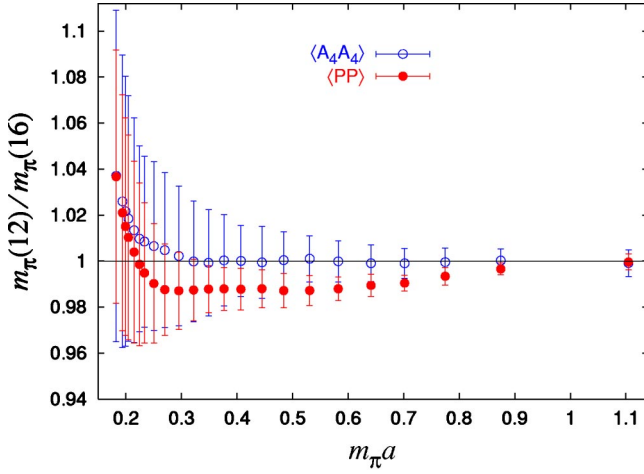
FIG. 16. Ratio of pion masses between the $12^2 \times 28$ and $16^3 \times 28$ lattices for both the $\langle A_4 A_4 \rangle$ and the $\langle PP \rangle$ correlators.

lattice sizes. It would be useful to compare the pion masses from $\langle PP \rangle$ and $\langle A_4 A_4 \rangle$ correlators to see how different they are in these cases.

To check the finite volume effect, we consider the pion mass from the $\langle A_4 A_4 \rangle$ correlator which is less affected by the zero mode contamination. We plot the ratio of pion masses between the $12^3 \times 28$ and $16^3 \times 28$ lattices in Fig. 16 as a function of m_π. We see that the ratio is basically unity for pion mass greater than ~ 300 MeV. Below this, the pion mass from the smaller volume, i.e. the $12^3 \times 28$ lattice, becomes higher. The worst deviation, at the smallest pion mass of 182(8) MeV, is 3.7%. For comparison, we also plot in Fig. 16 the corresponding ratio of m_π from the $\langle PP \rangle$ correlator. Contrary to the $\langle A_4 A_4 \rangle$ correlator, we see that the ratio has a dip between the m_π range of 250 and 800 MeV, again reflecting the fact that the pion mass calculated from the $\langle PP \rangle$ correlator on the $12^3 \times 28$ lattice has observable zero mode contributions.

To assess the finite volume correction, we first consider the leading finite volume correction calculated by replacing the infinite volume meson propagator with the finite volume counterpart. The correction [25] for m_π^2 is

$$\Delta(m_\pi^{1\text{-}loop})^2 = \frac{m_\pi^2}{4\pi^2 f^2}(\mu^2 - \alpha m_\pi^2)\sqrt{\frac{2\pi}{m_\pi L}}e^{-m_\pi L}, \quad (18)$$

where $\mu^2 = m_{\eta'}^2 - m_\eta^2/2 - m_{\pi 0}^2/2 = (871 \text{ MeV})^2$. With $\alpha m_\pi^2 \ll \mu^2$ [25], we can estimate the percentage difference of m_π^2 between the $12^3 \times 28$ and the $16^3 \times 28$ lattices for the smallest $m_\pi = 182(8)$ MeV to be

$$\frac{\Delta(m_\pi^{1\text{-}loop})^2(12) - \Delta(m_\pi^{1\text{-}loop})^2(16)}{m_\pi^2} = 0.13\%. \quad (19)$$

This is much smaller than the Monte Carlo calculation of 7.4% derived from the $\langle A_4 A_4 \rangle$ correlators in Fig. 16. Next, we use the empirical L^3 dependence [41] to estimate the finite volume correction with
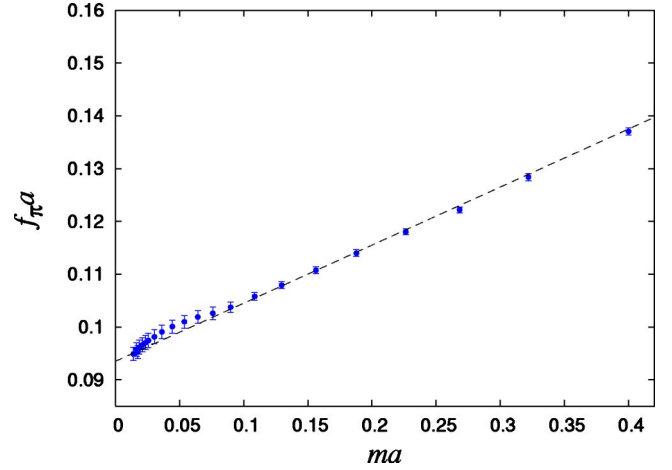

FIG. 17. f_π determined from the pseudoscalar correlator $G_{PP}(\vec{p}=0,t)$ in Eq. (21) as a function of the quark mass m. The dashed curve is a linear fit to the high mass region, $m = 0.1085$ [$m_\pi = 0.4438(36)$ or 438(7) MeV] to 0.4 [$m_\pi = 0.8740(30)$ or 862(13) MeV].

$$m_\pi(L) = m_\pi(L=\infty) + \frac{a}{L^3}. \quad (20)$$

For our lowest $m_\pi(L=16) = 182(8)$ MeV where the corresponding $m_\pi(L=12)$ is 3.7% higher, we obtain the finite volume correction for the $m_\pi(L=16) = 182(8)$ MeV to be 2.7% and the correction for $m_\pi^2(L=16) = [182(8)\text{MeV}]^2$ to be 5.4%. Similarly, for the second lowest pion mass at 193(7) MeV, the correction is 3.6% for $m_\pi^2(L=16)$. These are smaller than the statistical errors for the fitted low-energy parameters in Sec. IV.

We are not in a position to fully address the continuum limit extrapolation, as we only have results at one lattice spacing. However, we know there is no $O(a)$ error due to chiral symmetry [11] and the $O(a^2)$ and $O(m^2 a^2)$ errors are small [7,8,10]. We shall use the results from the small volume study in Ref. [8] to gain some feeling for the magnitude of the $O(a^2)$ errors. We have calculated pion and rho masses on the $6^3 \times 12$, $8^3 \times 16$, and $10^3 \times 20$ lattices with the Wilson gauge action at $\beta = 5.7$, 5.85, and 6.0 respectively. The figures of $m_\pi a/\sqrt{\sigma}a$ and $m_\rho a/\sqrt{\sigma}a$ (σ is the string tension) vs σa^2 in Ref. [8] show that both of them are quite flat at $m_\pi/m_\rho = 0.4$, 0.5, and 0.6. Since the lattice spacing at $\beta = 5.7$, as measured with the Sommer r_0, is 0.171 fm which is very close to our present lattice whose lattice spacing as determined from r_0 is 0.175 fm, we shall use the $\beta = 5.7$ data as the estimate for the present lattice. After extrapolating the pion mass from $\beta = 5.7$, 5.85, and 6.0 in Ref. [8] to the continuum limit, we find the central values of m_π at $\beta = 5.7$ are changed by 1%–3% for the cases with $m_\pi/m_\rho = 0.4$, 0.5, and 0.6. We thus tentatively suggest that our present pion masses are subject to the similar level of $O(a^2)$ errors due to the continuum limit extrapolation. This, of course, needs to be checked with calculations at smaller lattice spacings than what we have now.
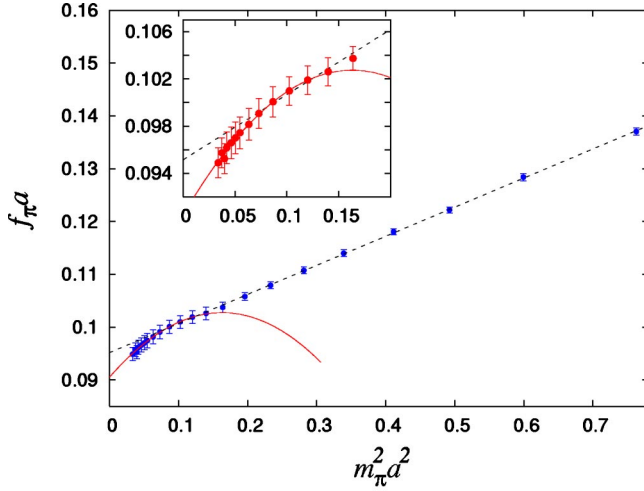
FIG. 18. f_π as a function of m_π^2. The dashed curve is a fit with $f_\pi(0) + C_1 m_\pi^2$ to the high mass region, $m_\pi = 0.4438(36)$ or 438(7) MeV to 0.8740(30) or 862(13) MeV. The solid curve is the fit with Eq. (22) for the small mass region, $m_\pi = 0.1844(71)$ or 182(8) MeV to $m_{\pi,max} = 0.3748(38)$ or 370(7) MeV. The inset is a blowup for the small mass region.

VI. CHIRAL BEHAVIOR OF f_π AND f_P

We show in Fig. 17 our data on renormalized f_π as obtained [10] from

$$f_\pi = \lim_{t \to \infty} \frac{2m\sqrt{G_{PP}(\vec{p}=0,t)m_\pi}e^{m_\pi t/2}}{(m_\pi)^2}. \qquad (21)$$

We see that if one fits a linear curve in quark mass from 0.1085 [$m_\pi = 0.4438(36)$ or 438(7) MeV] to 0.4 [$m_\pi = 0.8740(30)$ or 862(13) MeV] as is usually done in the literature, the fit gives $f_\pi = 0.0935(6) + 0.110(2)m$ with $\chi^2/N_{NDF} = 1.0$. In this case, the data below $m = 0.1085$ shows a hump with a one-sigma deviation from the linear fit at the low mass end. Even though f_π in full QCD with dynamical fermions has a leading order chiral logarithm [42,43] in the form $m_\pi^2 \log(m_\pi^2)$ with a known coefficient, it is absent in the
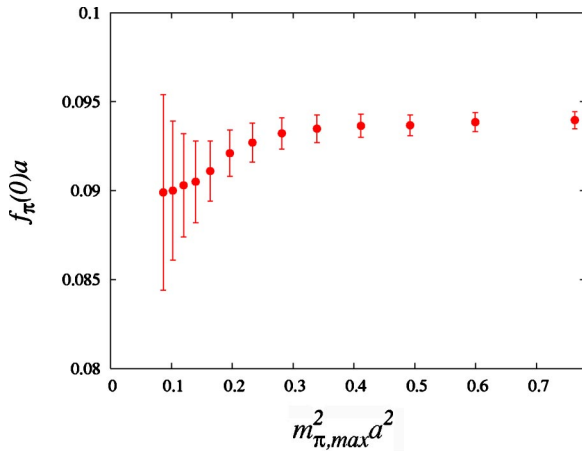

FIG. 19. $f_\pi(0)$ as determined from the fit Eq. (22) as a function of the maximum pion mass $m_{\pi,max}$.
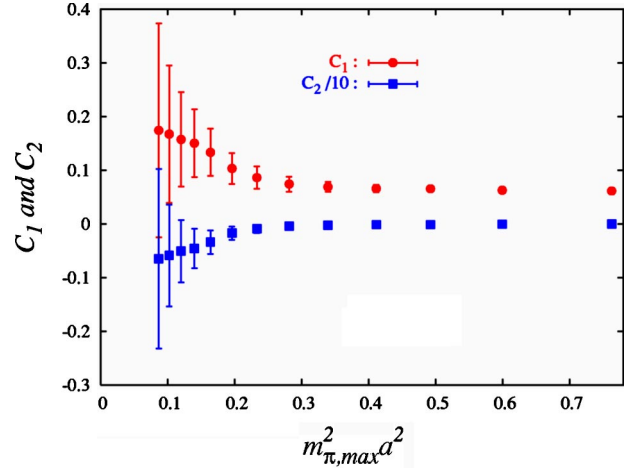

FIG. 20. Same as in Fig. 19 but for C_1 and $C_2/10$.

quenched theory [24]. We interpret the bump as a consequence of the quenched chiral logarithm in the pion mass. Thus, we plot the f_π as a function of m_π^2 in Fig. 18 and fit with the form

$$f_\pi = f_\pi(0) + C_1 m_\pi^2 + C_2 m_\pi^4. \qquad (22)$$

As in the fit of m_π^2, we fix the minimum pion mass at 0.1844(71) and fit the data to the above formula with variable ranges. The results of $f_\pi(0)$ are plotted in Fig. 19 as a function of the maximum pion mass $m_{\pi,max}^2$. We plot the same for C_1 and $C_2/10$ in Fig. 20. Even though there appear to be some changes in the region of $m_{\pi,max}$ between 0.3748(38) and 0.4840(32) for $f_\pi(0)$, C_1 and C_2, the errors are such that one cannot be as certain as in the case of the chiral logarithm δ. Thus, we shall quote the results for $m_{\pi,max} = 0.3748(38)$ or 370(7) MeV. They are given in Table VI. The fit for f_π in the range up to $m_{\pi,max} = 0.3748(38)$ with the parameters in Table VI is plotted in Fig. 18 as the solid lines for both the full figure and the inset. We also fit f_π with only the quadratic pion mass term for the large pion mass region from $m_\pi = 0.4438(36)$ or 438(7) MeV to 0.8740(30) or 862(13) MeV and obtain $f_\pi = 0.0952(6) + 0.0551(13)m_\pi^2$. This fit is plotted as the dash line in Fig. 18.

According to the quenched chiral perturbation theory [29], $C_1 = 4L_5/f_\pi(0)$. From our data reported in Table VI, we obtain $L_5 = 3.6(1.5) \times 10^{-3}$. This is comparable to $L_5 = 2.5(5) \times 10^{-3}$ as obtained from the study of f_π with the clover fermion action on Wilson gauge configurations at $\beta = 5.7$. But it is substantially larger than the phenomenological value of $1.4(5) \times 10^{-3}$ [44].

TABLE VI. $f_\pi(0)$, C_1, and C_2 as fitted from $m_\pi = 0.1844(71)$ or 182(8) MeV to $m_\pi = 0.3748(38)$ or 370(7) MeV.

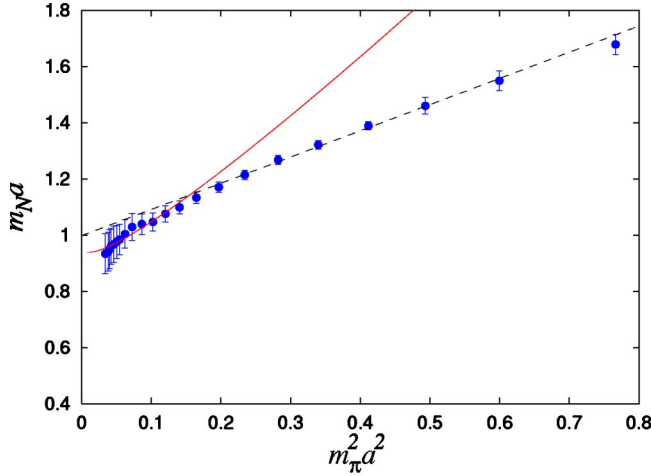| $f_\pi(0)$	C_1	C_2	L_5
0.0905(23)	0.150(63)	−0.46(37)	$3.6(1.5) \times 10^{-3}$

FIG. 21. The nucleon mass as a function of m_π^2. The dashed line is a fit only linear in m_π^2 for the range of m_π from 438(7) MeV to 862(13) MeV. The solid line is a fit with Eq. (27) for the range $m_\pi = 182(8)–316(6)$ MeV.

Using the experimental value $f_\pi(m_\pi) = 92.4$ MeV and $m_\pi = 137$ MeV to set the scale, we determine the lattice spacing a to be 0.200(3) fm. We see that $f_\pi(m_\pi)$ is higher than $f_\pi(0)$ by $\sim 5\%$.

The unrenormalized pseudoscalar decay constant of the pion is defined as

$$f_P^U = \langle 0 | \bar{\psi} i \gamma_5 (1 - D/2) \psi | \pi(\vec{p}=0) \rangle. \qquad (23)$$

From the chiral Ward identity, we have

$$Z_A \partial_\mu A_\mu = 2 Z_m m Z_P P, \qquad (24)$$

where $A_\mu = \bar{\psi} i \gamma_\mu \gamma_5 (1 - D/2) \psi$ and $P = \bar{\psi} i \gamma_5 (1 - D/2) \psi$. Since $Z_m = Z_S^{-1}$ and $Z_S = Z_P$ due to the fact the scalar density $S = \bar{\psi}(1 - D/2)\psi$ and the pseudoscalar density P are in the same chiral multiplet, Z_m and Z_P cancel in Eq. (24). Therefore, from the relation of the on-shell matrix elements

$$\langle 0 | Z_A \partial_4 A_4 | \pi(\vec{p}=0) \rangle = 2m \langle 0 | P | \pi(\vec{p}=0) \rangle, \qquad (25)$$

one obtains that

$$\frac{f_P^U}{f_\pi} = \frac{m_\pi^2}{2m}, \qquad (26)$$

where f_π is renormalized while f_P^U and m are unrenormalized. The relation also holds when both f_P and m are renormalized since $Z_m = Z_P^{-1}$. It is clear from Eq. (26) that the chiral behavior of f_P^U is the combination of those of $m_\pi^2/2m$ and f_π.

VII. QUENCHED m_N

We first plot the nucleon mass as a function of m_π^2 in Fig. 21. We see that it is fairly linear in m_π^2 all the way down to $m_\pi \sim 0.4438(36)$ [438(7) MeV]. Below that point, there appears to be a deviation from the linear behavior. Following
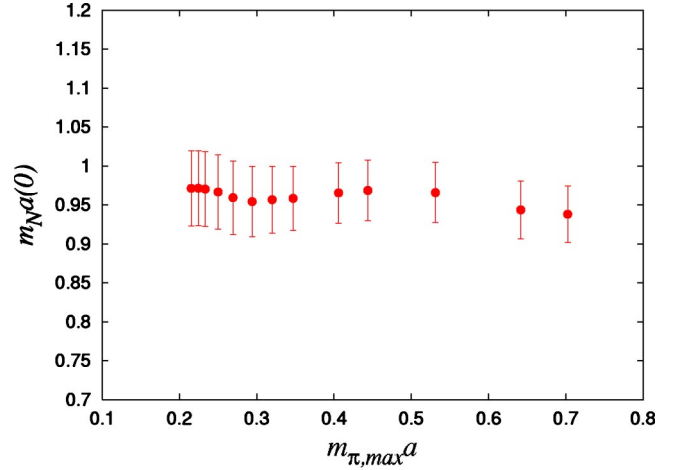

FIG. 22. Fitted $m_N(0)$ in Eq. (27) as a function of $m_{\pi,max}$ of the fitting range.

the case of f_π, we shall first fit the N mass only linear in m_π^2 in the range of $m_\pi^2 = 0.196–0.763$ and obtain $m_N = 0.998(21) + 0.932(74)m_\pi^2$. This fit is represented by a dashed line in Fig. 21. We see that the data (in the small m_π region) in this case are systematically lower than the linear fit.

According to the quenched χPT for the baryons [45], the one-loop result predicts the presence of the non-analytic terms m_π and $m_\pi^2 \log(m_\pi)$, both of which are proportional to the quenched δ. Thus, we fit the nucleon data from the lowest pion mass, i.e. $m_{\pi,min} = 182(8)$ MeV, upward as done in previous sections with the form

$$m_N = m_N(0) + C_{1/2} m_\pi + C_1 m_\pi^2 + C_{1L} m_\pi^2 \log\left(\frac{m_\pi}{\Lambda_\chi}\right) + C_{3/2} m_\pi^3. \qquad (27)$$

We should mention again that the fit does not depend on the value of Λ_χ, since there is an analytic term in m_π^2. We take $\Lambda_\chi = 1.16$ for this case.

The fitted results of $m_N(0)$ are plotted in Fig. 22 as a function of the maximum pion mass $m_{\pi,max}$ of the fitted range. We see that it is rather stable in the range fitted. Similarly, the coefficients $C_{1/2}$, C_{1L}, C_1 and $C_{3/2}$ are plotted in Fig. 23. We see that both $C_{1/2}$ and C_{1L} have rather smooth behavior in $m_{\pi,max}$ from 0.3 to 0.55 and approach zero around $m_{\pi,max} = 0.6–0.7$. On the other hand, C_1 has more of a variation in the range $m_{\pi,max} = 0.3–0.55$. When $m_{\pi,max}$ reaches the region 0.6–0.7, the error bars do not touch those at $m_{\pi,max} \sim 0.3$. We note that $C_{3/2}$ is consistent with zero in the whole range of the fit. We have tried to include the next analytic term m_π^4 [46]. It turns out that $m_N(0)$, $C_{1/2}$, and C_1 are not changed outside their errors in this case. However, $C_{3/2}$ and C_2 with the m_π^4 term become ill determined. They are consistent with zero but with large errors. Thus, the data seem to suggest that there is no evidence for a large m_π^3 term in the quenched nucleon mass. We quote the fit evaluated at $m_{\pi,max} = 0.3200(43)$[316(6) MeV] in Table VII. This fit is shown as the solid curve in Fig. 24 for m_π^2 up to
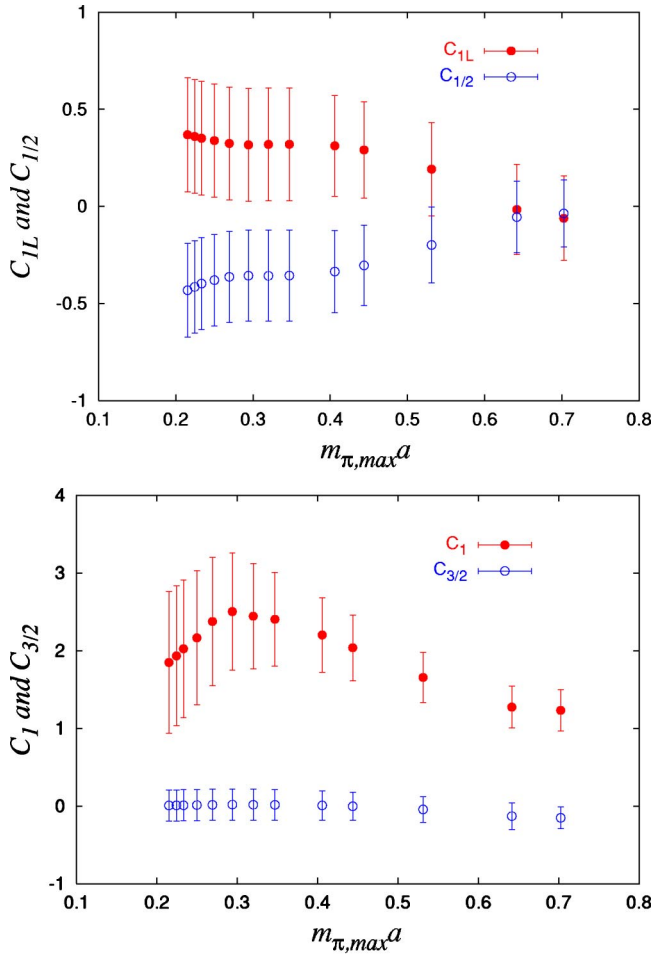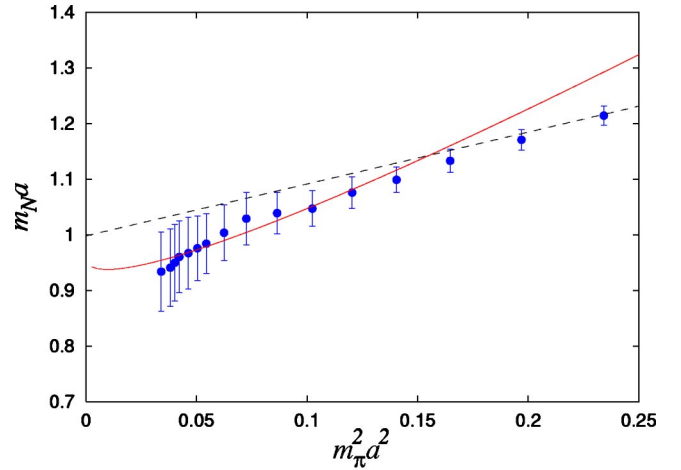
FIG. 24. The nucleon mass as a function of m_π^2 for smaller pion masses. The solid line is a fit with Eq. (27) for the range $m_\pi = 0.1844(71)[182(8)$ MeV$]$ to $0.3200(43)$ [316(6) MeV]. The dashed line is a linear fit from a higher mass range of $m_\pi = 0.4438(36)[438(7)$ MeV$]$ to $0.8740(30)$ [862(13) MeV].

FIG. 23. The same as in Fig. 22 for the coefficients C_{1L} and $C_{1/2}$ (upper figure) and for the coefficients C_1 and $C_{3/2}$ (lower figure).

$0.4840(32)[m_\pi = 478(8)$ MeV$]$. Also shown in the figure as the dashed curve is the linear fit from the higher pion mass range of $m_\pi = 0.4438(36)[438(7)$ MeV$]$ to $0.8740(30)$ [862(13) MeV].

We should mention that even though the error is large, $C_{1/2}$ is consistent with that predicted by the one-loop χPT [45], for which $C_{1/2} = -(3\pi/2)(D - 3F)^2 \delta$. Using $\delta = 0.20(3)$ from our fit in Sec. IV, it gives $C_{1/2} = -0.31(5)$. This is consistent with the value in Table VII which is $-0.358(234)$. Here $C_1 = 2.44(67)$ from the low mass fit is much larger than that of the high mass fit where $C_1 = 0.932(74)$.

VIII. CONCLUSION

The chiral extrapolation has always been a major challenge in lattice QCD calculations, primarily due to the fact

TABLE VII. $m_N(0)$, $C_{1/2}$, C_1, C_{1L}, and $C_{3/2}$ as fitted from $m_\pi = 0.1844(71)$ [182(8) MeV] to $0.3200(43)$ [316(6) MeV].

$m_N(0)$	$C_{1/2}$	C_1	C_{1L}	$C_{3/2}$
0.957(43)	$-0.358(234)$	2.44(67)	0.319(290)	0.016(199)

that one does not know if the formula used to fit is correct in the range of the available data. The idea of using χPT to guide the fit is useful and appropriate except it is complicated by the fact that one does not know the range in where the one-loop formula is valid. In this work, we attempt to answer this question by fitting the data from our smallest pion mass (close to the physical value) upward and seeing where the low-energy parameters change. This is commensurate with the χPT approach which expands around the small pion mass and momentum. The chiral logarithm δ from fitting the pion mass to the quenched one-loop chiral formula clearly demonstrates a sharp transition around 300–400 MeV in the pion mass. We take this as an evidence to reveal the upper limit for the applicability of the one-loop formula in quenched χPT. We have also fitted the pion mass with the cactus re-summed diagrams in quenched χPT and the results suggest that its range of applicability extends beyond the one-loop formula. We should point out that fitting with the cactus re-summed diagrams is preferred over the one-loop formula since it gives a scale-independent δ. However, not all the physical quantities have cactus re-summed results in the χPT and, in many cases, one would rely on one-loop formula to do the chiral fitting. Thus, it is essential to find out where the one-loop formula is valid. To be sure that this is not skewed by the finite volume effects, we compared our data on the $16^3 \times 28$ lattice against those on the $12^3 \times 28$ lattice and found that the finite volume errors are much smaller than the statistical errors. Although less certain due to larger errors, the analytic term in the N mass and in f_π shows variations in the pion mass range of 300–400 MeV, and the C_1 coefficients change by a factor of ~ 2–3 compared with those from fits involving exclusively pion masses beyond this range. Thus we tentatively conclude that the one-loop quenched χPT is valid for pion mass less than ~ 300 MeV. It is claimed that using a different regularization scheme such as the finite range regularization [47] will extend the range of validity for the one-loop quenched χPT

from that of the dimensional regularization, but it remains to be checked by lattice Monte Carlo data at low pion mass.

One of the valuable lessons learned in this study is that it seems futile to extrapolate to the chiral region from pion mass beyond ~ 300 MeV. We tried to fit the pion mass with the one-loop formula by extrapolating from $m_\pi = 862(13)$ MeV and found that, no matter how small pion masses one includes, δ is inevitably different (by more than two sigmas) from that obtained with the data limited to $m_\pi \lesssim 250$ MeV. One could try to model the functional form at higher masses, but it is not likely to succeed, because one does not know *a priori* how and when the modeled formula eases into that of the one-loop chiral χPT. Direct simulation at pion masses less than ~ 300 MeV is nearly impossible (or at the very least an extremely difficult task) for lattice calculations employing fermion actions which suffer from exceptional configurations and/or critical slowing down. An overlap-fermion calculation is numerically intensive, but with approximately fixed cost—its critical slowing down is rather mild [8]. The fact that it has chiral symmetry alleviates the worry that something may go wrong at small quark masses. Furthermore, the chiral behavior study is greatly enhanced by the incorporation of the multi-mass algorithm which facilitates the constrained curve-fitting method to discern the logarithm structure. One does not know how different the chiral behavior in full QCD will be from that of the quenched approximation, but it is hard to imagine that there are different scales for the sea and valence quarks. If so, one will need to work harder to lower the dynamical quark masses such that the corresponding pion mass is below ~ 300 MeV.

[1] C. Bernard *et al.*, hep-lat/0209086.

[2] For reviews, see, for example, H. Neuberger, Annu. Rev. Nucl. Part. Sci. **51**, 23 (2001); Nucl. Phys. B (Proc. Suppl.) **83-84**, 67 (2000); **73**, 105 (1999).

[3] R. Narayanan and H. Neuberger, Phys. Rev. Lett. **71**, 3251 (1993).

[4] R. Narayanan and H. Neuberger, Nucl. Phys. **B443**, 305 (1995).

[5] H. Neuberger, Phys. Lett. B **417**, 141 (1998).

[6] M. Lüscher, Phys. Lett. B **428**, 342 (1998).

[7] K.F. Liu, hep-lat/0206002.

[8] S.J. Dong, F.X. Lee, K.F. Liu, and J.B. Zhang, Phys. Rev. Lett. **85**, 5051 (2000).

[9] R.G. Edwards, U.M. Heller, and R. Narayanan, Phys. Rev. D **59**, 094510 (1999).

[10] S.J. Dong, T. Draper, I. Horváth, F.X. Lee, K.F. Liu, and J.B. Zhang, Phys. Rev. D **65**, 054507 (2002).

[11] Y. Kikukawa, R. Narayanan, and H. Neuberger, Phys. Lett. B **399**, 105 (1997).

[12] Y. Iwasaki, Nucl. Phys. **B258**, 141 (1985).

[13] H. Neuberger, Phys. Rev. D **57**, 5417 (1998).

[14] J. van den Eshof *et al.*, Comput. Phys. Commun. **146**, 203 (2002); Nucl. Phys. B (Proc. Suppl.) **106**, 1070 (2002).

[15] T.W. Chiu *et al.*, Phys. Rev. D **66**, 114502 (2002).

[16] E.I. Zolotarev, Zap. Imp. Akad. Nauk. St. Petersburg **30**, (1877).

[17] D. Ingerman, V. Druskin, and L. Knizhnerman, Commun. Pure Appl. Math. **53**, 1039 (2000).

[18] P.P. Petrushev and V.A. Popov, *Rational Approximation of Real Functions* (Cambridge University Press, Cambridge, England, 1987).

[19] R.G. Edwards, U.M. Heller, and R. Narayanan, Parallel Comput. **25**, 1395 (1999).

[20] H. Neuberger, Nucl. Phys. B (Proc. Suppl.) **83**, 813 (2000).

[21] R.G. Edwards and U.M. Heller, Phys. Rev. D **65**, 014505 (2002).

[22] T. Blum *et al.*, Phys. Rev. D **69**, 074502 (2004).

[23] W. Bardeen, A. Duncan, E. Eichten, N. Isgur, and H. Thacker, Phys. Rev. D **65**, 014509 (2002).

[24] S. Sharpe, Phys. Rev. D **46**, 3146 (1992).

[25] C. Bernard and M. Golterman, Phys. Rev. D **46**, 853 (1992).

[26] S. Sharpe, Phys. Rev. D **56**, 7052 (1997); **62**, 099901(E) (2000).

[27] J. Heitger, R. Sommer, and H. Wittig, Nucl. Phys. **B588**, 377 (2000).

[28] S. Aoki *et al.*, Phys. Rev. Lett. **84**, 238 (2000); CP-PACS Collaboration, S. Aoki *et al.*, Phys. Rev. D **67**, 034503 (2003).

[29] W. Bardeen, A. Duncan, E. Eichten, and H. Thacker, Phys. Rev. D **62**, 114505 (2000).

[30] QCDSF Collaboration, M. Göckeler, *et al.*, Nucl. Phys. B (Proc. Suppl.) **83**, 203 (2000).

[31] MILC Collaboration, C. Bernard *et al.*, Phys. Rev. D **64**, 054506 (2001); MILC Collaboration, C. Aubin *et al.*, hep-lat/0209066.

[32] S. Kim and S. Ohta, Phys. Rev. D **61**, 074506 (2000).

[33] Y. Aoki *et al.*, Phys. Rev. D **69**, 074504 (2004); RBC Collaboration, Y. Aoki, Nucl. Phys. B (Proc. Suppl.) **106**, 245 (2002).

[34] RGB Collaboration, C. Gattringer *et al.*, hep-lat/0209099; C. Gattringer, hep-lat/0208056; S. Hauswirth, hep-lat/0204015. We should note that the results quoted here are from a fitting method which includes nondegenerate quark masses.

[35] T.W. Chiu and T.H. Hsieh, Phys. Rev. D **66**, 014506 (2002); hep-lat/0208066.

[36] We will postpone the consideration of the finite volume effect and zero mode contribution to Sec. V.

[37] P. Lepage *et al.*, Nucl. Phys. B (Proc. Suppl.) **106**, 12 (2002).

[38] C. Morningstar, Nucl. Phys. B (Proc. Suppl.) **109**, 185 (2002).

[39] S.J. Dong, T. Draper, I. Horváth, F.X. Lee, K.F. Liu, N.

Mathur, C. Srinivasan, and J.B. Zhang (in preparation); S.J. Dong *et al.*, hep-lat/0208055.

[40] We thank S. Sharpe for explaining this to us.

[41] M. Fukugita *et al.*, Phys. Rev. Lett. **68**, 761 (1992); Phys. Lett. B **294**, 380 (1992); Phys. Rev. D **47**, 4739 (1993); S. Aoki *et al.*, *ibid.* **50**, 486 (1994).

[42] P. Langacher and H. Pagels, Phys. Rev. D **8**, 4595 (1973).

[43] J. Gasser and H. Leutwyler, Nucl. Phys. **B250**, 465 (1985).

[44] A. Pich, Rep. Prog. Phys. **58**, 563 (1995).

[45] J. Labrenz and S. Sharpe, Phys. Rev. D **54**, 4595 (1996); Nucl. Phys. B (Proc. Suppl.) **34**, 335 (1994).

[46] We thank D. Leinweber for pointing out the need to include the next analytic term in the chiral expansion.

[47] D. Leinweber, A. Thomas, and R. Young, Phys. Rev. Lett. (to be published), hep-lat/0302020.